Human Molecular Genetics, 2008, Vol. 17, No. 17 **2691–2702**
doi:10.1093/hmg/ddn171
Advance Access published on June 16, 2008

Als2 mRNA splicing variants detected in KO mice rescue severe motor dysfunction phenotype in *Als2* knock-down zebrafish

Francois Gros-Louis[1,2], Jasna Kriz[2], Edor Kabashi[1,3], Jonathan McDearmid[3], Stéphanie Millecamps[2], Makoto Urushitani[2], Li Lin[3], Patrick Dion[1], Qinzhang Zhu[4], Pierre Drapeau[3], Jean-Pierre Julien[2] and Guy A. Rouleau[1,*]

[1]Center for Excellence in Neuromics, CHUM Research Center and the Department of Medicine, University of Montreal, Montreal, QC, Canada, [2]Research Centre of CHUL (CHUQ), Department of Anatomy and Physiology, Laval University, Quebec, QC, Canada, [3]Department of Pathology and Cell Biology and Groupe de recherche sur le système nerveux central, Université de Montréal, Montréal, QC, Canada and [4]Institut de recherches cliniques de Montréal, Montréal, QC, Canada

Received January 23, 2008; Revised and Accepted June 6, 2008

Recessive *ALS2* mutations are linked to three related but slightly different neurodegenerative disorders: amyotrophic lateral sclerosis, hereditary spastic paraplegia and primary lateral sclerosis. To investigate the function of the *ALS2* encoded protein, we generated *Als2* knock-out (KO) mice and *zAls2* knock-down zebrafish. The *Als2*$^{-/-}$ mice lacking exon 2 and part of exon 3 developed mild signs of neurodegeneration compatible with axonal transport deficiency. In contrast, z*Als2* knock-down zebrafish had severe developmental abnormalities, swimming deficits and motor neuron perturbation. We identified, by RT–PCR, northern and western blotting novel *Als2* transcripts in mouse central nervous system. These *Als2* transcripts were present in *Als2* null mice as well as in wild-type littermates and some rescued the zebrafish phenotype. Thus, we speculate that the newly identified *Als2* mRNA species prevent the *Als2* KO mice from developing severe neurodegenerative disease and might also regulate the severity of the motor neurons phenotype observed in ALS2 patients.

INTRODUCTION

Amyotrophic lateral sclerosis (ALS) is a common, usually fatal, adult-onset neurodegenerative disorder characterized by degeneration of motor neurons in the cortex, brainstem and spinal cord (1). Dysfunction and death of these cell populations leads to progressive muscle weakness, atrophy and, ultimately, paralysis and death within 3–5 years after onset (2). Despite several genetic advances, the actual cause and mechanism of neurodegeneration in ALS remains a mystery. Although most of the reported cases are sporadic (SALS), ~10% are familial (FALS) and, of these, ~10–20% are caused by mutations in a gene encoding the metalloenzyme Cu/Zn superoxide dismutase-1 (*SOD1*) (3,4). More recently, mutations in a second gene (*ALS2*) were shown to cause a recessive and juvenile onset form of the disease (5,6). The *ALS2* gene encodes a protein having multiple motifs with homology to the guanine-nucleotide exchange factor (GEF) (for review see 7). To date, there are over 120 different missense mutations that have been reported (http://www.alsod.org) in the *SOD1* gene and 12 in the *ALS2* gene. *ALS2* gene mutations all lead to either ALS, where both upper/lower motor neurons are affected, or to primary lateral sclerosis (PLS) or infantile onset ascending hereditary spastic paraplegia (IAHSP), where only upper motor neurons are affected (5,6,8–13).

The *ALS2* gene is comprised of 34 exons spanning 80 kb of human genomic DNA on chromosome 2q. An *ALS2* transcript

*To whom correspondence should be addressed at: Ste-Justine Hospital Research Center and The Center for Excellence in Neuromics 1560, rue Sherbrooke est, Y-3633 Montreal, QC, Canada H2L 4M1. Tel: +1 5143454740/5148908000 Ext. 24699; Fax: +1 5143454698/5144127602; Email: guy.rouleau@umontreal.ca

contains an open reading frame (ORF) of 6.4-kb, which is predicted to encode a 184 kDa protein consisting of 1657 amino acids known as the long form of alsin. A second transcript (2651 bp) contains a shorter ORF of 1191 nucleotides, which encodes a shorter form of alsin (396 amino acids), has also been described (5,6). To date, the molecular features of alsin have not been experimentally determined and mechanisms by which loss of its function leads to a selective dysfunction and disease-related degeneration of motor neurons remain unknown. Furthermore and somewhat paradoxically, no overt phenotype consistent with ALS or other motor neuron disease were present in *Als2* knock-out (KO) mouse generated by different groups (14–18).

In order to investigate the function of alsin, we have generated *Als2* KO mice ($Als2^{-/-}$) of our own. Our mice, such as all previously described *Als2* KO models (14–18) developed rather normally and showed only a mild motor neuron phenotype. Since little is known about the expression pattern and subcellular localization of alsin, we generated polyclonal antibodies against alsin. Using these antibodies, we have shown that alsin is ubiquitously expressed in most neurons throughout the central nervous system (CNS). We have also identified, by RT–PCR, northern and western immunodetections, novel *Als2* transcripts in both mouse and human tissues. Finally, we have generated a zebrafish model in which the *zAls2* gene expression was knocked down using antisense morpholino oligonucleotides (AMO) designed to prevent translation of its mRNA. In contrast with *Als2*-deficiant mice, z*Als2* knock-down embryos showed a severe motor neuron phenotype and developmental abnormalities. This phenotype was rescued by injection of both full-length and novel *Als2* mouse transcript. Our zebrafish model is the first animal model mimicking the severe motor neuron ALS phenotype and may provide a new tool to better understand this yet untreatable disease.

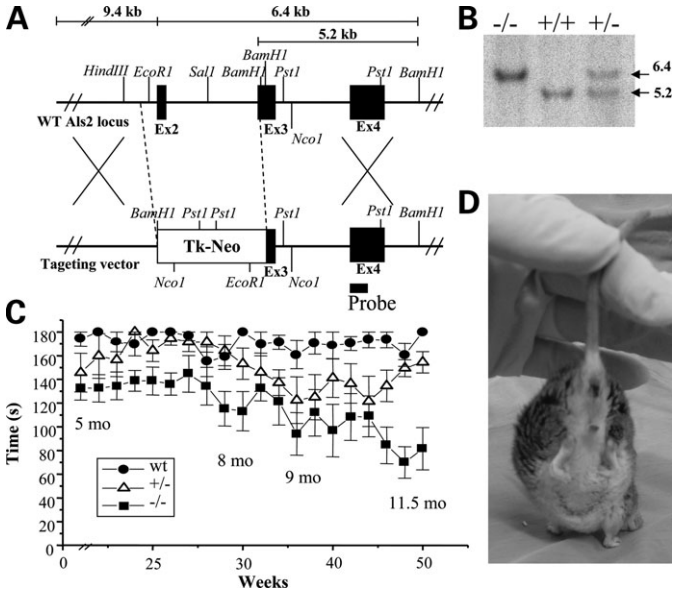

Figure 1. Targeted disruption of the *Als2* KO mice. (**A**) Restriction enzyme maps of the WT Als2 locus and the targeting vector. The coding exons of the *Als2* gene are indicated by black boxes. ES cell clones were detected by a probe located in exon 4 outside the targeting vector (black bar). (**B**) Analysis of genomic DNA from $Als2^{-/-}$ animals by Southern blot. The *Bam*H1 fragments detected for WT (5.2 kb) and targeted (6.4 kb) *Als2* alleles. (**C**) Motor performance of WT ($n = 15$), $Als2^{+/-}$ ($n = 13$) and $Als2^{-/-}$ ($n = 14$) mice on accelerating rotarod. Data are presented as means and SD at different time points. (**D**) $Als2^{-/-}$ mouse showing modest decrease in grasping test and abnormal limb flexions when lifted by the tail.

RESULTS

Evidence of pathological changes in *Als2* null mice

To generate a mouse model of ALS2, we constructed a targeting vector designed to replace exon 2 and a part of exon 3 with a neo cassette (Fig. 1A). This targeting vector was transfected by electroporation into R1 embryonic stem (ES) cells (129/SV strain) and clones were selected according to their ability to grow in a neomycin environment. ES cell clones that carried the homologous recombination event with expected *Bam*HI bands of 9.4 and 6.4 kb (Fig. 1A) were microinjected into C57BL/6 blastocysts to generate chimeric mice. The $Als2^{-/-}$ mice were derived by inbreeding of different strains, 129/SV and C57BL/6, in order to derive F1 heterozygous $Als2^{+/-}$ mice. Southern blotting of mouse DNA confirmed the generation of mice homozygous for the null *Als2* gene (Fig. 1B). Homozygous *Als2*-deficient mice were generated by crossbreeding heterozygous mice.

At birth, the *Als2* KO mice had no obvious defects motor or morphological deficits and were of normal size, compared with their wild-type (WT) littermates (data not shown). However, as they got older, the *Als2* KO mice developed signs of mild motor dysfunction when challenged by an accelerating rotarod. The motor deficits started to be more prominent at 8 months of age and their performance slowly declined till 12 months of age when it stabilized. Interestingly, about the same time point, the *Als2* heterozygous mice showed a tendency to develop slight motor deficits, however, the values were not significantly different compare with WT littermates (Fig. 1C). These animals also presented with a modest decrease in muscle strength test (70.9 ± 3.7 g for *Als2* KO, 86.8 ± 14.6 g for heterozygous mice and 104.5 ± 14.1 g for WT littermates $n = 6$) and sometimes abnormal limb flexions when lifted by the tail (Fig. 1D). In addition, quantitative analysis of the total number of motor axons at 8 months of age revealed a slight decrease in the numbers of motor axons in L5 ventral roots of *Als2*-deficient mice (787 ± 37 *Als2* KO versus 935 ± 23 for the WT littermates, $n = 4$). Further immunohistological analysis revealed no signs of microglial activation or reactive astrocytosis in the spinal cord section of *Als2* KO mice (data not shown).

The overt phenotypes observed in our *Als2* null mice were less severe and more subtle than anticipated from human ALS2-related disorders. Nonetheless, electron microscopy (EM) provided evidence of pathological changes in nerve fibres lacking *Als2*. In 18-month-old *Als2* null mice, EM revealed a high number of degenerating axons in corticospinal tracts (Fig. 2B). The most striking abnormality was that the periaxonal space of myelinated motor axons was frequently dilated (Fig. 2B, D and F). This was observed in myelinated axons of both the sciatic nerve as well as of CNS corticospinal tracts from the *Als2* null mice, but not from normal littermates. In addition, EM showed evidence of accumulations of membranous organelles in paranodal areas of axons (Fig. 2H).

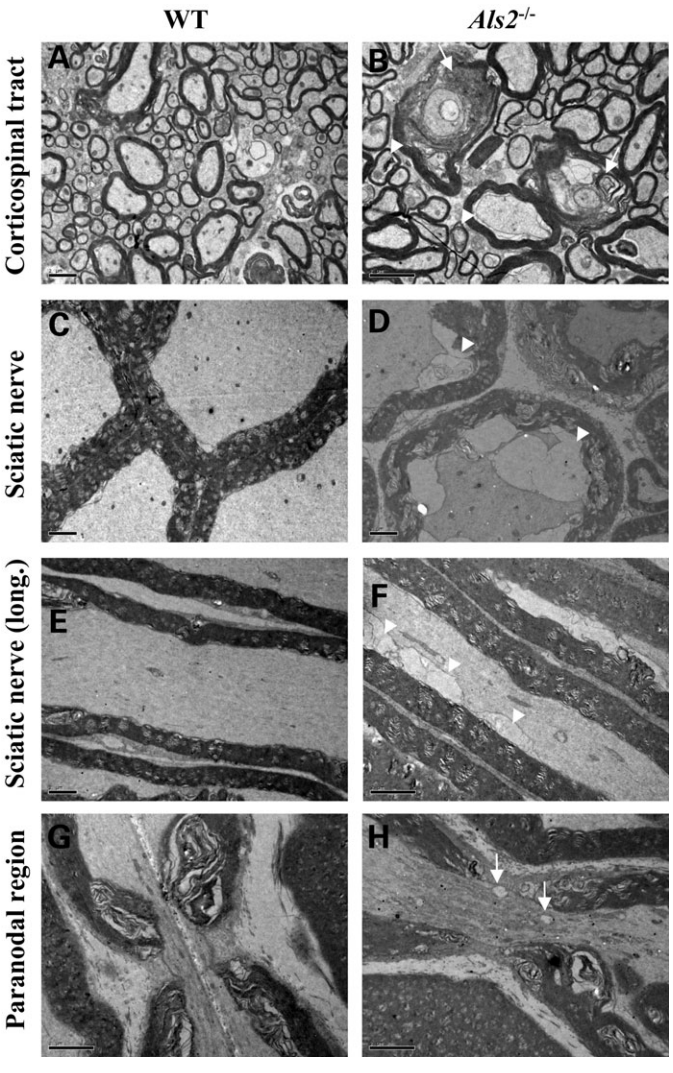

Figure 2. Electron microscopy analysis of *Als2* KO mice and WT littermates. Degenerating axons (arrows) and dilated periaxonal space (arrowheads) in corticospinal tract and sciatic nerve of *Als2* null mice (**B, D** and **F**), but not in WT (**A, C** and **E**). Accumulations of organelles in paranodal region of axon lacking alsin (**H**; arrows) compared with WT littermate (**G**).

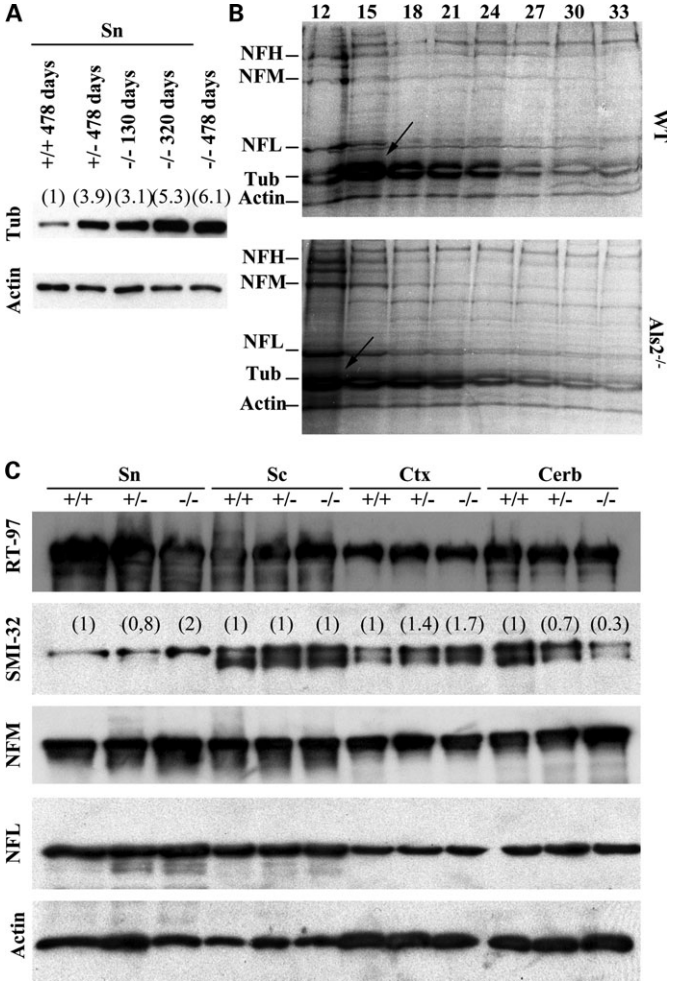

Figure 3. Western blot analysis of *Als2* expression in various tissues of WT (+/+), heterozygous (+/−) and homozygous *Als2* KO mice (−/−) using Al-7 antibody. (**A**) Total protein extracts (10 μg) from sciatic nerve immunoblotted with BIII-tubulin antibody showing enhance level of tubulin in aging animals. The numbers between brackets represent the relative expression level of tubulin after normalization with actin. (**B**) *In vivo* neurofilament transport studies in sciatic nerves revealing axonal transport impairments in *Als2* null mice. L5 ventral, dorsal roots and dorsal root ganglia were pooled in one fraction (12) and protein extracts were loaded on the lane 1. Consecutive 3-mm segments (15–33) of the sciatic nerve were loaded in each successive lane of the gel extending distally to the right. Positions of NF-H (200-kDa), NF-M (150-kDa), NF-L (68-kDa), tubulin (55-kDa) and actin (45-kDa) are indicated. A slower rate of transport of [35S]-methionine-labelled tubulin is seen in the sciatic nerve in normal mice than in *Als2* null mice (arrows). (**C**) Immunoblot of extracts from the sciatic nerve (Sn), spinal cord (Sc), cortex (Ctx) and cerebellum (Cerb) showing abnormal expression of neurofilament NF-H unphosphorylation detected with SMI-32 antibody in sciatic nerve, cortex and cerebellum. Normal expression level of phosphorylated NF-H (RT-97), NF-M and NF-L proteins in *Als2* null mice were also detected. Actin staining reflects the level of gel loading in all panels. The numbers between brackets represent the relative expression level of tubulin after normalization with actin.

Interestingly, axonal transport also seems to be impaired in KO animals as immunoblotting, after SDS–PAGE of tissue extracts, revealed increased levels of tubulin in the sciatic nerve of *Als2* null mice (Fig. 3A). This abnormality was detected in 130 days of age KO animals and tended to increase with age. Following these observations, the transport of cytosqueleton proteins was measured *in vivo* to evaluate the distal migration of tubulin, neurofilaments NF-L, NF-M and NF-H in 4-month-old $Als2^{-/-}$ animals and their WT littermates. This was done separately, at different time intervals, following the physical migration of [^{35}S]-methionine radiolabelled intermediate filament and microtubule proteins from their injection site in the spinal cord through the ventral root and ultimately the sciatic nerve (19). No difference was observed when we compared the transport of NF-L, NF-M and NF-H of $Als2^{-/-}$ and WT animals (Fig. 3B). However, during the same period of time, the peak of [^{35}S]-methionine radiolabelled tubulin migrated more distally in the sciatic nerve of normal mice than $Als2^{-/-}$ mice (Fig. 3B) indicating slower axonal transport. The detection of western blots using SMI-32 antibody, which selectively detects the unphosphorylated form of NF-H, showed an abnormal reduction of this protein in the whole lysates prepared from the cerebellum (Fig. 3C). This was accompanied by a slight increase of the same

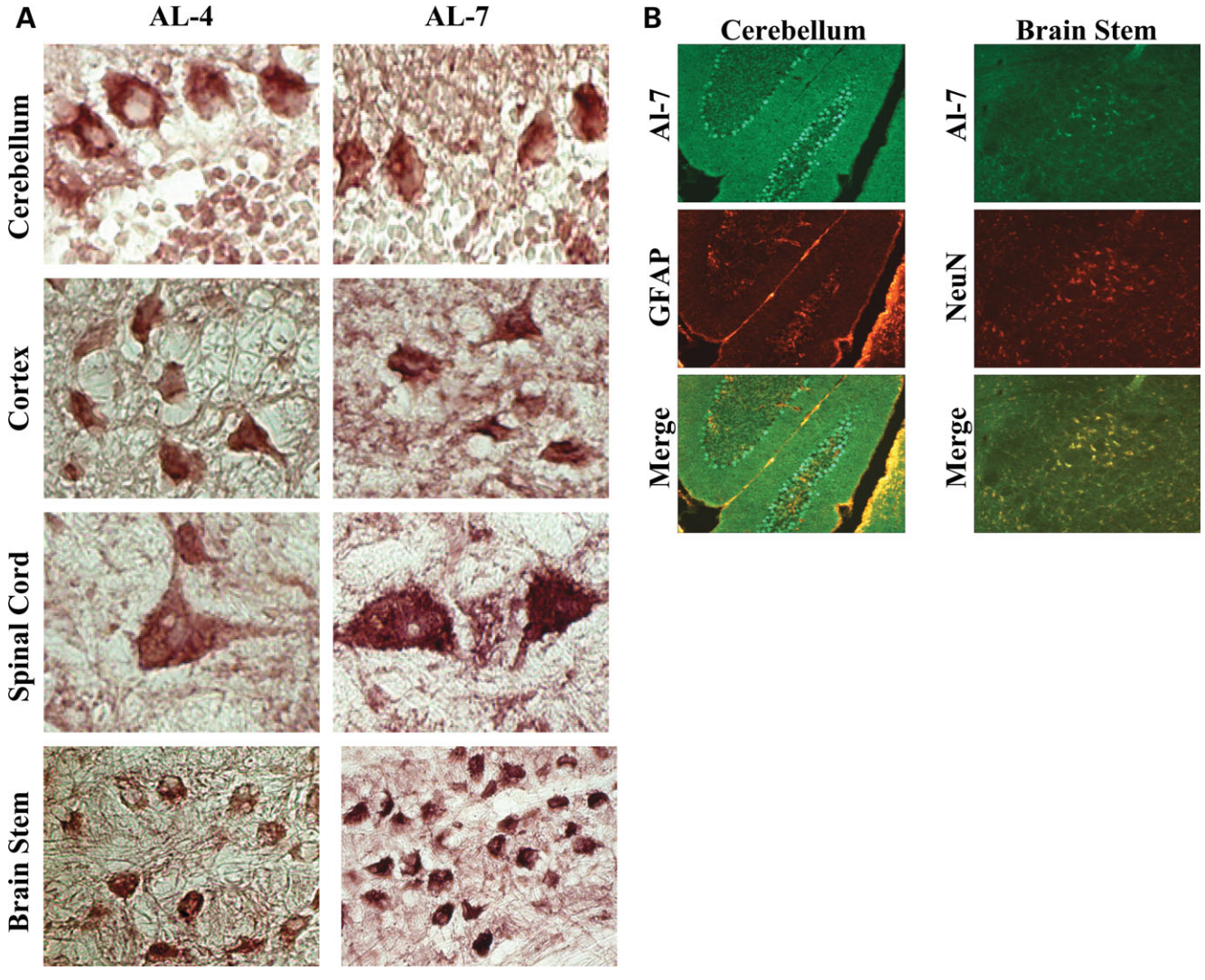

Figure 4. Immunohistochemistry showing that Als2 is ubiquitously expressed in neurons throughout the CNS in WT animals ($Als2^{+/+}$). (**A**) Each brain or spinal cord section was immunostained with the AL-4 and the AL-7 antibodies. (**B**) Co-immunostaining in different brain region of alsin (AL-7 antibody in green) and either glial fibrillary acidic protein (GFAP) or neuronal nuclei (NeuN) markers in red. The lower panel represent the merge between the two upper panels and shows that alsin is expressed in neurons and not in glial cells.

protein in the sciatic nerve and the cortex of the same animals (Fig. 3C). Expression of the other two neurofilaments, NF-L and NF-M, and the levels of phosphorylated NF-H (RT-97 antibody) appeared to be unaffected in $Als2^{-/-}$ mice (Fig. 3C).

Alsin is a 180-kDa protein with many other isoforms and is expressed in neurons

Immunohistochemical analysis of the mouse Als2 protein using either Al-4 or Al-7, Als2-specific rabbit polyclonal antibodies generated for this project, combined with neuronal (NeuN) and glial (GFAP) markers showed that the Als2 protein is expressed in various neurons throughout the CNS, but not glia (Fig. 4). Both immunohistochemistry and western blots indicated that alsin was expressed in the CNS with the highest level of expression detected in the brain stem, cerebellum and spinal cord (Fig. 5E). Taken together, these findings confirm the previously reported expression pattern of *Als2* mRNA (5). The Als2 protein in non-CNS tissues was expressed at lower levels when compare with those detected in the brain except in skeletal muscle cells and in the heart where high expression was observed (Fig. 5F). We also confirmed that alsin is expressed during embryonic development using mouse embryo protein extracts (E13.5) (Fig. 5E).

A major common band of ~180-kDa was detected, using anti-sera raised against the C-terminal part of alsin (AL-7), in mouse and human tissues (Fig. 5D–F). This band was not present in protein lysates of cultured lymphoblast cells from patients homozygous for mutations in the *ALS2* gene (Fig. 5D) and was also not detected in brain tissue from an *Als2* KO mouse (Fig. 5E). The 180-kDa band is consistent with the predicted long form of alsin. We also detected several additional bands. In particular, a ≈66-kDa band that was abundant in both WT and *Als2* KO neuronal mouse tissues as well as in heterozygous carriers and normal

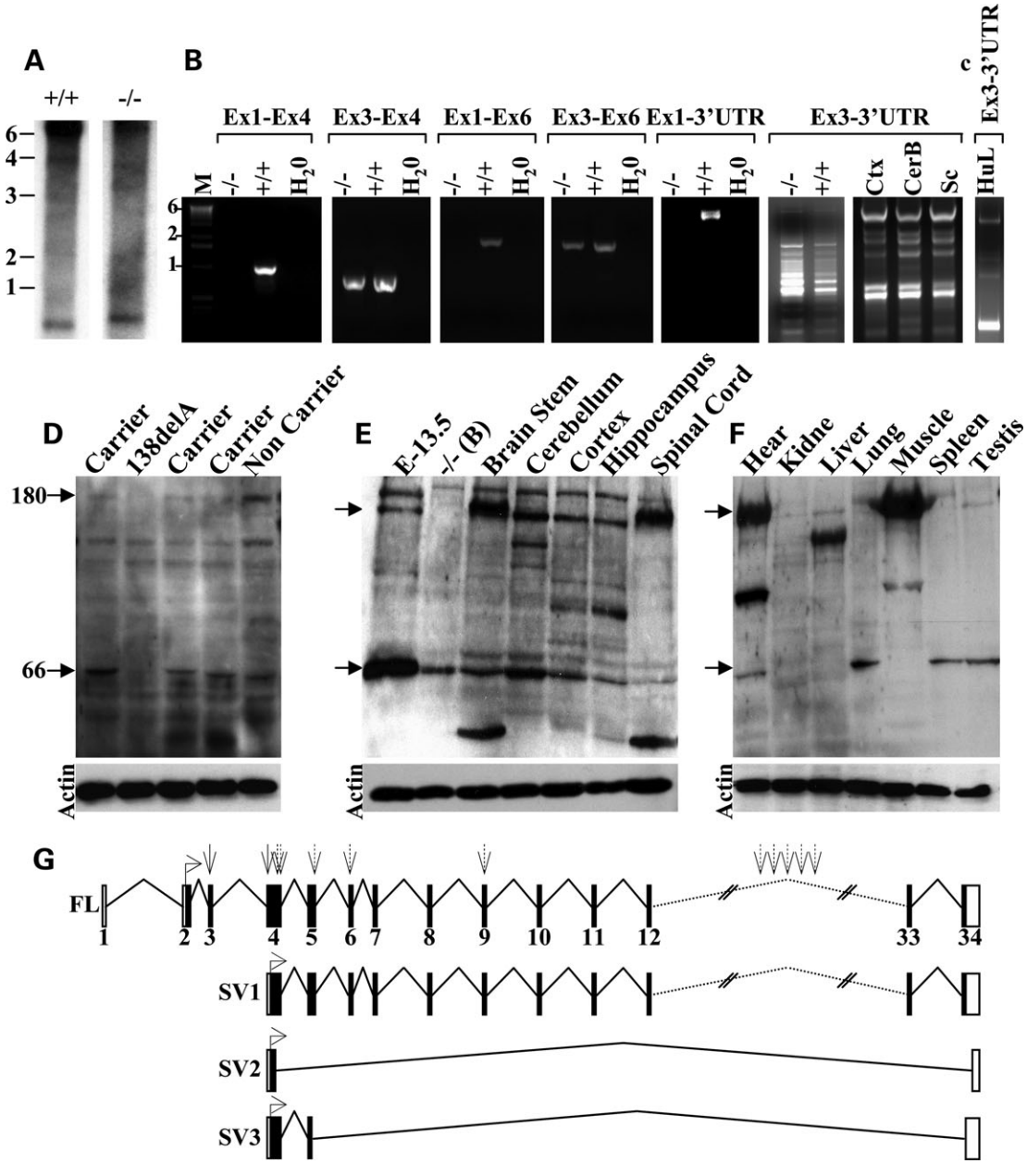

Figure 5. Molecular characterization of novel *Als2* transcripts. (**A**) Northern blot analysis from polyA RNA extracted form brain of WT (+/+) and *Als2* null mice (−/−) showing the presence of multiple *Als2* mRNA species. (**B**) RT–PCR analysis from brain cDNA of WT and *Als2* null mice using different combinations of primers specific for the mouse *Als2* gene. The first panel shows 1-kb DNA ladder (M), the absence of *Als2* cDNA product after PCR amplification using primers in exon 1 and in exon 4 located, respectively, upstream and downstream the *Bam*H1 recombination site (see Fig. 1) in *Als2* mull mice conversely to WT littermates, confirming that full-length *Als2* was successfully knocked out. The second panel reveals the presence of *Als2* cDNA product after PCR amplification using primers in exon 3 and 4 both located downstream the recombination site, confirming that some *Als2* mRNA species are still transcribed. Results presented in the third to fifth panels confirm the results presented in the first two panels. The sixth panel shows the presence of multiple *Als2* mRNA transcripts after PCR amplification using primers located in exon 3 and in the 3′-UTR in both WT and *Als2* null mice. The seventh panel illustrates also the presence of multiple *Als2* mRNA transcripts after PCR amplification using primers located in exon 3 and in the 3′-UTR in WT mice using cDNAs made from brain cortex (Ctx), cerebellum (CerB) and spinal cord (Sc). (**C**) RT–PCR from transformed human lymphoblastoid cell line (HuL) showing the presence of different *ALS2* transcript. (**D**) Werstern blot analysis using total protein extract from human ALS2 lymphoblastoid cell lines and from different neuronal (**E**) and non-neuronal (**F**) mouse tissues. The blots presented in this figure have been immunostained with the AL-7 C-terminus antibody. Note the absence of full-length *ALS2* in patients and full-length *Als2* in mice and, the presence of other *ALS2*/*Als2* isoforms, including a 66-kDa band absent in one ALS patient. Note also that the pattern of expression of the *Als2* isoforms was different depending on the tissues examined. The black arrows indicate the 180-kDa full-length *Als2* and the 66-kDa *Als2* isoform. These arrows act also as migration marker for each of the blots presented in this figure. (**G**) Schematic diagram of four different *Als2* mRNA, including the full-length (FL) *Als2*, the longest alternative *Als2* species (SV1) and the shortest *Als2* specie (SV2 and SV3). The black boxes represent the exons, the black lines illustrate each of the splicing event between exons and the dotted interrupted lines represent only gap to facilitate and lighten this schematic representation. Straight filled arrows represent the location of reported ALS-linked ALS2 mutations and straight dotted arrows represent the location of IAHSP- or PLS-linked ALS2 mutations. The angulated arrows represent the ATG start codons.

individuals but absent in a patient homozygous for the 138delA mutation (Fig. 5D). We cannot exclude the possibility that some of the faint bands may be the results of cross reactivity of the antibody with other peptides. However, we believe that many of the major bands detected are real alsin isoforms, particularly the 66-kDa band which were absent in an ALS2 patient.

Identification of other *Als2* isoforms in mouse tissues

In order to confirm the absence of full-length alsin in *Als2* KO mice and to establish whether other cross-reacting products detected by western blot analysis, in particular the 66-kDa bands, were actually the result of novel splice isoforms of alsin, we performed RT–PCR and northern blot analysis (Fig. 5A and B). As expected, when using an *Als2* specific set of PCR primers designed in the first exon of the *Als2* gene (forward primer) and in the exon 6 or 3′-UTR (reverse primers), no transcripts corresponding to the *Als2* gene were detected by RT–PCR when using cDNA generated from *Als2* KO brain tissues (Fig. 5B). However, when using PCR primer pair designed to amplify the region between *Als2* exon 3 (downstream the *Bam*H1 cloning and recombination site, see Fig. 1A) and exon 6, RT–PCR amplification products were detected in both $Als2^{-/-}$ animals and WT littermates (Fig. 5B). To search for new *Als2* transcripts, we analyzed the poly(A) RNA fraction of mouse brains ($Als2^{-/-}$ and WT littermate) by performing RACE–PCR and nested PCR amplifications. Different *Als2* cDNAs were isolated using the same PCR primer pair designed downstream to the *Bam*H1 recombination site and 3′-UTR region (Fig. 5B). The same pattern of RNA expression was also seen in different brain regions (cerebellum, cortex and spinal cord) suggesting that there are no specific alsin transcripts found in these specific brain regions. All the amplified cDNAs were cloned in TOPO-T/A vector (Invitrogen) and their subsequent sequencing showed that they all corresponded to unreported isoforms of *Als2* in both KO animals and WT littermates (Fig. 5F and Supplementary Material, Fig. S1). Northern blot analysis using two specific probes designed to recognize the 3′ untranslated region of the *Als2* transcript also revealed the presence of several mRNA species, confirming our RT–PCR results (Fig. 5A). The different band sizes are likely to be the result of alternative ATG transcription initiation sites and/or alternative splicing events. A detailed analysis of the *Als2* sequence (NM_028717) demonstrated the presence of an 'inframe' possible alternative ATG, at position 340 located in exon 4 (position number 1 being the 'A' of the principal initiation transcription site located in exon 2). This ATG was found in all newly identified *Als2* transcripts (Fig. 5G and Supplementary Material, Fig. S1). In mouse, the pattern of expression of these different *Als2* mRNA species seems to be different in various mouse tissues as bands of different size were found on western blots (Fig. 5E and F). These different Als2 gene products were not detected using pre-immune anti-sera (data not shown). RT–PCR experiments using PCR primer pairs specific for human exon 3 and 3′-UTR revealed the presence of multiple *ALS2* cDNA species using mRNA made from human lymphoblastoid cells (Fig. 5C).

Morpholino-mediated knock-down of *zals2* in zebrafish

In parallel to our $Als2^{-/-}$ mouse model, we also generated z*Als2* knocked down zebrafish in which the translation of the z*Als2* gene was blocked by an AMO. In contrast to the scenario observed in all *Als2* KO mice generated to date (including the one reported here), knock-down of the z*Als2* gene expression in zebrafish led to a severe developmental and behavioral phenotype that resulted in swimming defects (Fig. 6B and F). This phenotype was apparent in 1–4-day-old AMO-microinjected larvae. AMO-injected fish failed to survive to the fifth day of development. To exclude the possibility that this phenotype may have resulted from non-specific or mistargeting effects of the AMO, we injected zebrafish embryos with a control 5-bp mismatch AMO. As expected, all control AMO-microinjected larvae developed normally and no apparent phenotype was observed (Fig. 6A and E). These data suggest that the phenotype observed with AMO-microinjected embryos was a direct result of alsin protein abrogation. To quantify the knock-down of z*Als2* AMO-injected larvae, western blots of protein extracts from these z*Als2* larvae and control AMO-treated larvae were compared. The generated Al-7 polyclonal antibody detected a band in western blots from zebrafish whole protein lysates corresponding to the predicted molecular weight of z*Als2* in control embryos (Fig. 6I). This band was not detected in z*Als2* knocked down embyos, confirming the knock-down of the z*Als2* gene (Fig. 6I).

To further confirm the specificity of our z*Als2* knock-downs, we performed rescue studies by microinjecting zebrafish larvae with a z*Als2*-specific AMO along with the full-length WT mouse *Als2* mRNA that was not targeted by the zebrafish-specific AMO. As shown in Figure 6C and G, full-length mouse *Als2* mRNA partially rescued the *zAls2* knock-down phenotype. We also attempted to rescue the AMO-microinjected z*Als2* knock-down with an alternative *Als2* mRNA species (SV1, see Fig. 3G) in order to determine if some of the novel *Als2* transcripts observed in the mouse were functional. The partial rescue of the *zAls2* knock-down phenotype with the SV1 *Als2* mRNA suggests that this particular *Als2* mRNA is functional and may modulate the phenotype in the $Als2^{-/-}$ mice (Fig. 6D and H). The frequency of tail contractions during touch-evoked swimming episodes was also quantified showing a significant decrease in tail contractions in z*Als2* knock-downs when compared to larvae injected with control AMO (Fig. 6J). The decreased frequency of tail contraction was also partially rescued by WT full-length and SV1 *Als2* mRNA (Fig. 6J). Each of the injected larvae was also scored visually for developmental defects, motor deficits or abnormal behaviors (Fig. 6K).

We next used immunohistochemical methods to determine neuroanatomical changes induced by z*Als2* knock-down. Immunohistochemical detection using an antibody specific for alpha-acetylated tubulin neurons labelling a range of neuronal processes, including motor neurons, revealed an obvious deficit in motor neuron projections in z*Als2* knock-downs (Fig. 6F, white arrow). Furthermore, spinal cords of AMO-microinjected larvae appeared to be abnormally developed (Fig. 6F). We additionally used an antibody against the pan-neuronal protein HU to quantify the number of differentiated neurons in the larval spinal cord (20). Anti-HU staining revealed

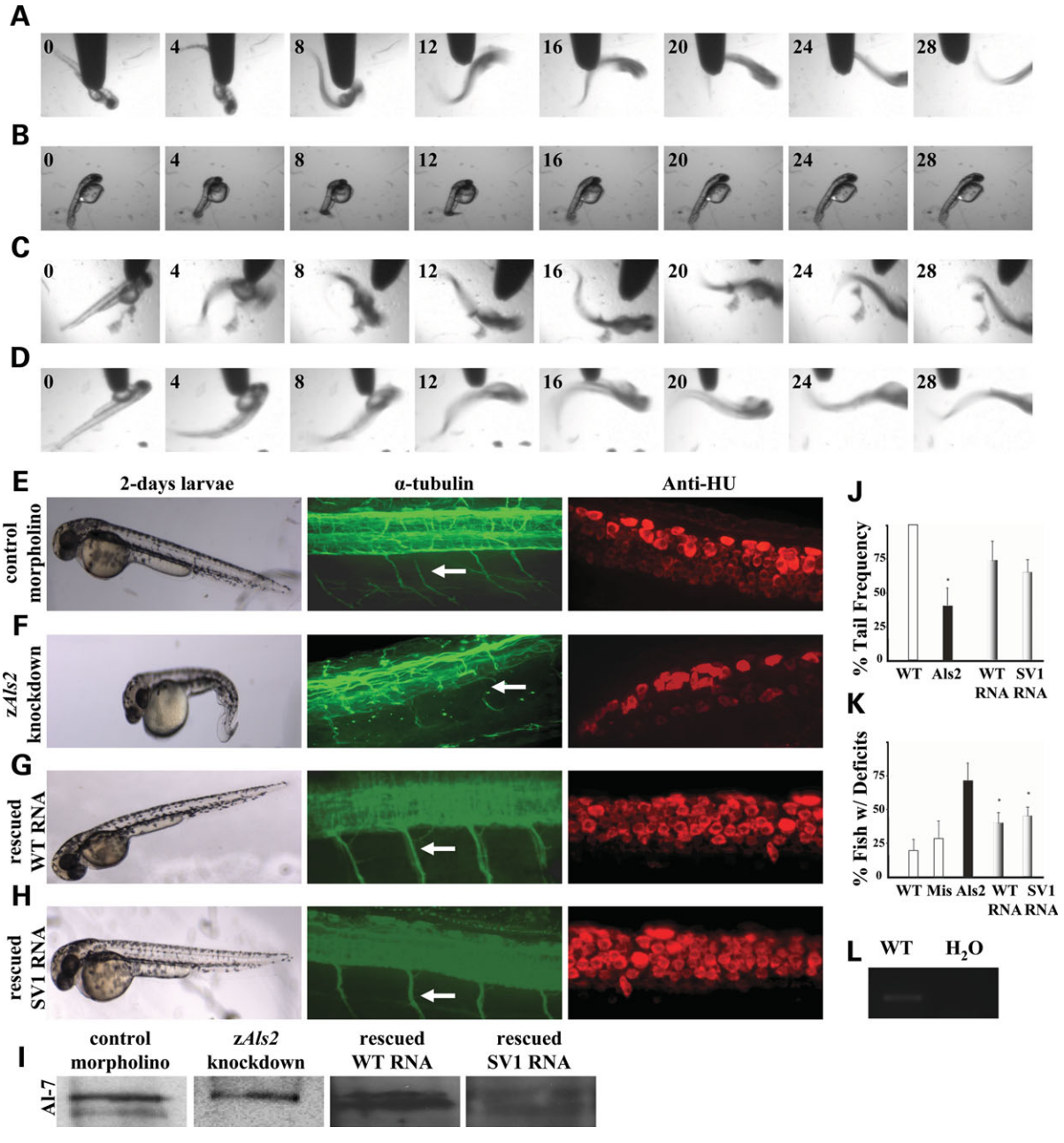

Figure 6. AMO-mediated knock-down of the z*Als2* gene. (**A**) 2-day-old larvae injected with control 5-bp mismatch AMO. Touch-evoked escape response illustrated by head to tail contractions. The swimming response was recorded at the indicated times (in milliseconds) after the stimulus. (**B**) 2-day-old larvae injected with z*Als2* AMO. Note the lack of touch-evoked escape response and the development problems in z*Als2* knock-down larvae. The response was recorded at the indicated times (in milliseconds) after the stimulus. (**C**) 2-day-old larvae injected with z*Als2* AMO and mouse FL *Als2* mRNA. Touch evoked-escape responses in z*Als2* knock-down rescued larvae. The response by z*Als2* knock-down rescued embryo was recorded at the indicated times (in milliseconds) after the stimulus. (**D**) 2-day-old larvae injected with z*Als2* AMO and mouse SV1 *Als2* mRNA. Touch evoked-escape responses in z*Als2* knock-down rescued larvae. The response by z*Als2* knock-down rescued embryo was recorded at the indicated times (in milliseconds) after the stimulus. (**E**–**H**) 2-day-old larvae injected either with control morpholino (E), with z*Als2* specific AMO (F) with z*Als2* AMO with FL mouse *Als2* (G) and z*Als2* AMO with SV1 mouse *Als2* isoform (H). All the panels illustrate typical observed phenotype in injected embryos. Motor neurons (white arrows) were stained with anti-tubulin antibody. Note pathfinding and abnormal motor neurons projection and z*Als2* KD fish. This phenotype is completely rescued while injecting the z*Als2* knock-downs with different *Als2* transcripts indicating the biological importance of these transcripts. Early differentiated neurons stained with anti-HU antibody from various z*Als2* knock-downs showing that z*Als2* is necessary for early development of zebrafish embryos. (**I**) Western blot results, using alsin-specific Al-7 antibody. Two different molecular weight bands were detected in 1-day and 2-day-old embryos. The higher molecular weight band is most likely a cross-reacting non-specific band as it was also detected using pre-immune anti-serum (data not shown). The lower band most likely represents alsin, which has been successfully knocked down. (**J** and **K**) Quantification of different z*Als2* knock-downs ($n = 100$ for each groups); The frequency of tail contraction was determined following a touch-evoked escape response from 2 days post-fertilization zebrafish non-injected, injected with a mismatch morpholino (white bars), injected with a specific z*Als2* morpholino (black bars), co-injected with z*Als2* AMO and WT full-length mouse *Als2* RNA, co-injected with Als2 morpholino and SV1 mouse *Als2* isoform (grey bars) (J). These fishes were also scored visually for developmental and motor deficits (K). (**L**) RT–PCR results, using cDNA made from zebrafish WT larvae, showing the presence on only one alsin isoform.

a significant decrease ($P \leq 0.001$) in the number of HU-positive neurons in AMO-injected larvae (z*Als2* knock-down: mean of 31.7, SD of 5.6, $n = 8$) (control: mean of 67.9, SD of 4.5 $n = 8$) (Fig. 6E and F). Both the motor neuron aberrant projections and the decrease of HU-positive neurons detected in AMO-microinjected larvae were not observed in rescued larvae (Fig. 6G and H) confirming that WT full-length *Als2* as well as SV1 *Als2* mRNA are functional. Finally, only one band of expected size was amplified by RT–PCR when using cDNA made from zebrafish larvae (Fig. 6L). Since similar PCR conditions were used all along this study and specific PCR primer pairs to the z*Als2* orthologous gene were used, it is likely that this band corresponds to z*Als2* cDNA.

DISCUSSION

We report the generation of two vertebrate models to study the loss of function of the *Als2* gene. Despite an age-dependent loss of motor coordination revealed by rotarod and grip strength performances of the *Als2* KO mice, no overt motor neuron degeneration was observed in the *Als2*-defecient mice we generated. Five other independent groups have also generated *Als2* mouse KOs (14–18). Similar to our findings, all these mouse models largely failed to recapitulate classical hallmarks of motor neuron disease. All *Als2*-deficient mice appear to be grossly normal, viable and fertile with lifespan expectancy similar to WT littermates. Some discrepancies are noteworthy and may explain the heterogeneity of the subtle phenotype observed in each mouse models. The diversity of apparent phenotypes among different alsin-deficient mouse models may be due in part by different the gene-targeting strategies used to generate each mice models, ES cell lines used leading to differences in the genetic background, housing conditions or approaches taken to evaluate the mice. However, unlike the $Als2^{-/-}$ KO mouse models, the z*Als2* knock-down zebrafish exhibited severe motor dysfunction. The data presented here suggest that the moderate phenotypes of the $Als2^{-/-}$ KO mice generated to date by different laboratories (14–18) is likely related to the existence of functional mRNA species despite disruption of the targeted *Als2* gene.

Although targeted disruption of the *Als2* gene in mice did not reveal striking signs of neurodegeneration, some interesting phenotypes were nonetheless observed. EM revealed the presence of degenerating axons in corticospinal tracts as well as accumulations of membranous organelles in paranodal areas of axons. Furthermore, the periaxonal space of myelinated motor axons was frequently dilated suggesting the appearance of a myelin disorder. These observations also suggest that an axonal transport defect may occur in ALS2 and indeed, the distal transport of tubulin in the sciatic nerve of $Als2^{-/-}$ animals was found to be altered. Moreover, enhanced expression of tubulin was found in the sciatic nerve of *Als2* null mice. This abnormal expression of tubulin also seemed to increase with age. Nevertheless, it is difficult to establish at the moment a cause to effect with this up-regulation of tubulin and motor impairment observed in the $Als2^{-/-}$ mice. Interestingly, the *Als2* heterozygous animals presented an intermediate phenotype observed when the mice were challenged with an accelerating rotarod and on the muscle strength analysis. This intermediate phenotype is also observed at the molecular level where intermediate expression of tubulin and unphosphorylated NF-H was found in heterozygous animals, suggesting a gene dosage effect. These changes are however not sufficient to induce pathology in mice.

Our $Als2^{-/-}$ mouse model enabled us to discriminate and characterize a number of novel *Als2* isoforms expressed in the nervous system by RT–PCR, northern blot and western blot analysis. Taken together, our results strongly suggest that other alternatively spliced *Als2* isoforms may exist and that some of these novel *Als2* mRNA species still can be transcribed in *Als2* null animals and may exert an unknown function partly compensating for the loss of the full-length isoform. Consistent with this hypothesis, the knock-down of the zebrafish *Als2* orthologue, using an AMO directed against the start codon of the z*Als2* gene, led to both severe developmental abnormalities and an obvious behavioral phenotype, including swimming impairment and motor neuron disruption mimicking the human disease. This phenotypic observation was absent in control animals and thus seems to be a direct result of the knocking down of zebrafish alsin expression, which was confirmed by western blot using rabbit polyclonal Al-7 antibody shown to react with the z*Als2* gene product. Alternative pre-mRNA splicing is widely used by higher eukaryotes to generate different protein isoforms in specific cell or tissue types. Human brain, testis and liver have been previously reported to be the site of unusually high levels of alternative splicing events (21). The frequency of alternative splicing is also believed to relate to organism complexity (22) and might explain such difference in the phenotypic severity between $Als2^{-/-}$ mice and knock-down z*Als2* zebrafishes. In agreement, no other isoforms were detected by RT–PCR when using RNA extracted from WT zebrafish larvae. Based on our results, it would be of great interest to design a new approach to generate an *Als2* KO mouse in which all splice isoforms are deleted. The Cre/loxP system would be an excellent alternative to targeted disruption to generate a mouse model in which all *Als2* splice isoforms would be successfully knocked out in order to elucidate the alsin function and to bring new insights in the pathogenic mechanisms involved in this disease.

Very little is known about the function of alsin. It is believed, since the protein contains multiple motifs homologous to GEFs, that alsin may exert some GEFs function. Currently, it has been shown that alsin may play a role in endocytic trafficking and axonal outgrowth (23–25). The interplay and the dynamic relations between the sub-domains encoded by the C-terminal part of *Als2* appear to be crucial in regulating Rab5 activity. It was demonstrated that a fragment of alsin containing a diffuse B cell lymphoma homology and pleckstrin homology like domain (DH/PH) interacts specifically with Rac1 a Rho GTPase (24). Rho family proteins are involved in the organization of the actin cytoskeleton and vesicle trafficking. Rab proteins act as membrane organizers that are also involved in vesicular transport and, specifically, the VPS9 domain within alsin, suggested by the interaction with Rab5, may be required for endosome fusion and endosome motility (23,26). Interestingly, the z*Als2* AMO-injected

fish showed a severe spinal cord phenotype characterized by abnormal motor neuron outgrowth in the spinal cord, suggesting that alsin might be implicated in motor axon pathfinding and so be important in early development. The C-terminal domains of alsin are likely to be of important physiological relevance in mediating the rescue effects observed in our zebrafish Als2 model as only the DH/PH and VPS9 domains with the membrane occupation and recognition nexus motifs are present in the SV1 *Als2* splice variants. The relationship between these domains are still unclear but, based on our results, it is likely that these domains are necessary to promote endocytic trafficking and axonal outgrowth. Thus, loss of alsin associated GEF function, which may results in the obstruction of membrane trafficking and dynamics, could underlie neuronal dysfunction and motor neuron degeneration seen in our zebrafish model.

The loss of function approach in zebrafish provided, for the first time, *in vivo* evidence that z*Als2* is not only required for global embryonic development and growth but may also play a specific functional role in cell migration and motor neuron development or maintenance. Conversely to what have been found in *Als2* knocked out mice, the phenotypic defects observed our *in vivo* zebrafish model are consistent with the ALS2 phenotype, suggesting that the presence of extra *Als2* mRNA species might exert a biological effect protecting these mice from developing ALS. Considering the lack of severe motor neuron deficit in all other published *Als2* mice model, in which different targeting strategies were used and where either exon 2, exon 3 or part of exon 4 have been targeted to specifically inactivate the gene (14–18), we propose that the alternative ATG start codon located in exon 4 is functional, producing the described splice variants. Western blot analysis as well as immunohistochemistry experiments also showed that alsin is ubiquitously expressed in various mouse tissues. The selective loss of motor neurons, in the face of widespread expression, suggests a critical role in maintaining the integrity of these large metabolically active cells. Surprisingly, the highest level of alsin expression was seen in Purkinje cells of the cerebellum and in the inferior olivary nucleus of the brain stem, and it might not be irrelevant that some ALS2 patients have marked cerebellar atrophy (27). However, it is not clear whether or not there is cerebellar ataxia in ALS2 patients as degeneration of motor neurons may mask such symptoms.

Interestingly, some of the novel *Als2* mRNA species were also detected in lymphoblastoid cell lines derived from an IAHSP ALS2-linked patient, suggesting a possible role in modifying the ALS phenotype. Different *ALS2* mutations may cause either ALS, where both upper/lower motor neurons are affected, or to PLS, or IAHSP, where only upper motor neurons are affected. The pattern of inheritance and the nature of all the ALS-linked mutations suggest that the phenotypes result from a loss of function. However, it is interesting to note that ALS-linked *ALS2* mutations are all located prior to the alternative ATG start codon, while all IAHSP- or PLS-linked *ALS2* mutations are all downstream this alternative start codon (Fig. 4G). This suggests that some of the *ALS2* mRNA, as found in the *Als2* KO animals and in ALS2 patient lymphoblast cells, might still be transcribed and attenuate the phenotype from ALS (more severe) to HSP or PLS (less severe), predicting functional differences between the full and short isoforms. This phenotype/genotype correlation will impact on the interpretation of diagnostic testing and may give insights on function/phenotype. Our results, with respect to the ability of both full-length *Als2* and truncated novel *Als2* transcript to rescue motor phenotype, also indicates a potential therapeutic benefit of alternate *Als2* transcripts. Gene therapy in ALS2-linked diseases may be an important avenue that it is worth exploring.

MATERIALS AND METHODS

Generation of a mouse with targeted disruption of *Als2*

The first step towards the generation of a KO mouse was the isolation of genomic clones for *Als2*, which was achieved by PCR amplification using the following oligonucleotides: (5′-AATCAGCAGAAATTTGTCCAAGCAG-3′ cDNA (position 341–365) and 3′-TACCACCGTGTTCTCAAACACC TCT-5′ cDNA (position 1008–984) from the published sequence. For screening and Southern hybridization, we made a DNA probe corresponding to the beginning of *Als2* exon 4. The screening of a 129/SV mouse strain genomic library from the TCAG-Genome Resource Facility (Toronto) led to the isolation of two BAC clones. The mapping of these two BAC clones was established by Southern blot analysis and the gene identification was confirmed by DNA sequencing. Two *Bam*HI fragments containing exon 2 and exon 3 amd 4 from one of the BAC clones were subcloned into the *Bam*HI site of pQZ1BamHI, a pUC-derived vector and the exon/intron join regions were sequenced. Examination of the restriction map of the *Als2* gene was subsequently performed, and we decided to create a targeting vector where exon 2 and part of exon 3 would be replaced by a 1.1 kb neo cassette (Fig. 1A). This DNA targeting vector was transfected by electroporation into R1 ES cells (129/SV strain) and neomycin-resistant colonies were selected as previously described (28). ES cell clones that carried the homologous recombination event with expected *Bam*HI bands of 9.4 and 6.4 kb (Fig. 1A) were microinjected into C57BL/6 blastocysts to generate chimeric mice. Male chimeras were separately mated with normal female mice of a 129/SV, a C57BL/6 or a mixed background of the two previously mentioned strains. The $Als2^{-/-}$ mice were derived by inbreeding of different strains, 129/SV and C57BL/6, in order to derive F1 heterozygous $Als2^{+/-}$ mice. Southern blotting of mouse DNA confirmed the generation of mice homozygous for the null *Als2* gene (Fig. 1B).

Rabbit polyclonal antibodies generation

Synthetic peptides were cross-linked to keyhole limpet haemocyanin, emulsified in Freund's adjuvant, and used to immunize two rabbits with each peptide (1.0-mg in complete Freund's adjuvant for the first injection, followed every 4–6 weeks by 0.5-mg in incomplete Freund's adjuvant). Based on their antigenicity and hydrophobicity, two oligopeptides (Al-4: MD SKKRSSTEAEGSKERGLV and Al-7: RIRNLGSEVHLI EDLMDP) were generated against specific regions of the protein. Serum from immunized rabbits were first screened

using ELISA showing a good immunological response from each rabbits (data not shown). AL-4 and AL-7 were chosen for use in immunostaining experiments.

Western blots

WT C57BL/6 mice, *Als2* KO mice and WT littermate (7–22 months of age) were killed by cervical dislocation; the dissected tissues (brain, spinal cord, heart, liver, kidney, spleen, muscle and testis) were rapidly frozen in liquid nitrogen and stored at −80°C until used for RNA or protein extraction.

Whole protein lysates from mouse and human tissues were extracted by homogenization of the tissues in SUB lysis buffer (0.5% SDS, 8 M Urea, 2% β-mercapto-ethanol in water), and centrifugation for 20 min at 13 000 r.p.m. at 10°C. The soluble protein was quantified by the Lowry method and diluted in loading buffer (15% glycerol, 5% SDS, 80 mM Tris–HCl, pH 6.8, 5% β-mercapto-ethanol and 0.01% bromophenol blue). Each sample (70 μg) was run on a 10% SDS/glycine polyacrylamide gel and then transferred electrophoretically to a nitrocellulose membrane (Schleicher & Schuell, Dassel, Germany). The blots were blocked in 5% non-fat milk/0.1% Tween 20 in phosphate-buffered saline (PBS) and probed with the generated antibodies diluted 1:500 in the blocking buffer. Immunodetection was performed with a donkey anti-rabbit-HRP-labelled secondary antibody (Jackson ImmunoResearch Laboratories ins.), and the detection was performed with the Renaissance kit (PerkinElmer Life Sciences, Boston, MA, USA). The blots were then re-probed with an anti-actin antibody to document equal loading. Quantification of western blots was carried out using ImageJ software and normalization against actin and WT mouse ($Als2^{+/+}$) for each tissue considered was then calculated. A number of commercially available primary antibodies were also used in this study namely, the monoclonal antibody against NF-L (nr4; 1:2000) was purchased from Novo Castra, NF-M (nn18) and NF-H (RT-97) (1:10 000 and 1:5000, respectively) were purchased from Chemicon, β-tubulin (1:2000) and anti-actin (1:10 000) monoclonal antibodies were purchased from Sigma. SMI-32 (1:2000) antibody came from Sternberger Monoclonals Inc.

Electron microscopy

Mice were perfused with 3% glutaraldehyde in PBS, pH 7.4. Tissues were incubated in 2% osmium tetroxide in 0.1 M PBS, dehydrated in a graded ethanol series and embedded in Epon. The ultrathin sections (60–90 nm) were cut using Reichert-Jung Ultracut E ultramicrotome, collected on Nickel/formvar grids and stained with uranyl acetate and lead citrate for microscopic observations.

Immunohistochemistry

Mice were anaesthetized by intraperitoneal injection of 4% chloral hydrate and perfused intracardially with PBS, followed by 4% paraformaldehyde, pH 7.4, in 0.1 M sodium phosphate buffer. Different tissues including brain, kidney, heart, liver, lung, muscle, spleen, spinal cord and testis were removed, post-fixed for 1 h, and then frozen in Tissue-Tek OCT embedding compound (Sakura Finetek, Torrance, CA, USA). Immunocytochemistry was performed on 12-μm thick sections. Sections were first quenched in 0.3% H_2O_2 for 30 min, permeabilized in 1% Tween 20 for 10 min, blocked in 3% normal goat serum for 3 h, and then incubated with the primary anti-ALS2 antibodies for 16 h at room temperature. Visualization was made by incubating the slides with a biotinyled goat anti-rabbit secondary antibody (Dako). The anti-ALS2 polyclonal antibody was generated in our laboratory. Co-localization studies were performed using anti-GFAP (1:1000) and NeuN (1:500) monoclonal antibodies both purchased from Chemicon. Secondary Alexa Flour® 594 goat anti-mouse (1:250) were purchased from Molecular Probes.

Zebrafish embryos were dechorionated and anaesthetised in 0.02% tricaine (Sigma) and subsequently fixed in 4% paraformaldehyde dissolved in phosphate buffer for 2 h at room temperature or overnight at 4°C. After extensive washing, embryos were permeabilized for 30 min with distilled water and incubated 1 h in blocking solution (2% goat serum, 1% bovine serum albumin, 1% dimethylsulfoxide, 0.1% Triton X-100 in PBS). Fixed embryos were incubated overnight at room temperature in primary antibody diluted in blocking solution. Primary antibodies used were anti-Hu (1:50; Molecular Probes), anti-acetylated tubulin (1:100; Sigma). Embryos were washed with PBSTx (0.1% Triton X-100 in PBS) and incubated overnight at room temperature in Alexa 488- or Alexa 568-conjugated secondary antibodies diluted in blocking solution (1:750; Molecular Probes). After rinsing in PBSTx, embryos were incubated in 50% glycerol in PBS and mounted on coverslips. Imaging was performed using an Ultraview LCI confocal microscope with Metamorph imaging software (PerkinElmer, Woodbridge, ON, USA).

Reverse transcriptase polymerase chain reaction

Total RNA was extracted from various mouse tissues or from human ALS2 lymphoblastoid cell cultures using TRIZOL reagent (Invitrogen) according to the manufacturer's protocol. Complimentary DNA synthesis was done using a standard protocol with oligo-dT primers and Moloney murine leukaemia virus reverse transcriptase. Different set of PCR primer pairs, designed from mouse mRNA (NM_028717), were used in this study: 5′-UTR forward primer (5′-GAGAGCT TTTGCTAATGGGATGG-3′), exon 3 forward primer (5′-CA GCCCGTCATTAGCAGTTAGGAT-3′), exon 4 reverse primer (3′- ACTGCCCCATGAGTAAACCTGAG-5′), exon 6 reverse primer (3′-ACTTGGTCTTTTCCTGGGGTGTTG-5′) and 3′-UTR reverse primer (3′-CCCACCCCCACCCCTAGCAAAG TA-5′). PCR primer pairs designed from human *ALS2* mRNA (NM_020919) were used: exon 3 forward primer (5′-CCTGC AGCCCCGCCCTGTCC-3′) and 3′-UTR reverse primer (3′-TC CTAGCAGCTCAGAGTCGGTGTC-5′). Finally, PCR primer pair designed from zebrafish were also used in this study (forward primer: 5′-TCGTGACGGAGGATGGAGGAGTG-3′ and reverse primer: 3′-TTGAGCAATGGCTGGAGCAGAA GA-5′). PCR amplification of each newly synthesized cDNA was done using the same touchdown PCR conditions as previously described (29).

Northern blots

Total RNA was extracted from various mouse tissues with TRIZOL reagent (Invitrogen) according to the manufacturer protocol. Poly(A) RNA was then purified from 0.50 to 0.75 mg of total RNA using Quiagen oligotex system. Poly A^+ RNA from *Als2* KO mice and WT littermates were separated on agarose gel and blotted with two different *Als2*-specific P32-radiolabelled DNA probes. The probe was generated by PCR amplification of cDNA synthesized from total RNA using *Als2*-specific PCR primer pairs (5′-CTGGAGGCTGA TGGGGCAAAGAAC-3′ and 3′-CCCACCCCCACCCCTAG CAAAGTA-5′).

Axonal transport

As previously described (19) the L-[^{35}S]-methionine, 1 μl (250 μCi/μl) (1175 Ci/mmol; PerkinElmer Life Sciences) was injected into the anterior horn area, 1 mm deep from the dorsal surface and 1 mm from the middle groove, at a rate of 0.5 μl/min delivered by a syringe pump (KD Scientific, New Hope, PA, USA). Mice ($n = 3$ per group) were deeply anaesthetized by intraperitoneal injection of 75 mg/kg xylazine and 10 mg/kg ketamine. Back muscles were carefully incised to expose the laminae of vertebra. Under an operating microscope, a 1–2 mm^2 window was drilled in the right lamina, at the level of L5 spinal cord, with a small electric drill (Dremel MultiPro, Rotary Tool 395T6 model, Racine, WI, USA) to expose the right spinal cord without damage. After injection the muscles were closed in layers with silk sutures and the skin incision was closed by wound suture clips. One hour after waking, the mice were administered a subcutaneous injection of 0.1 mg/kg buprenorphine (Reckitt & Colman Pharmaceuticals, Inc., Richmond, VA, USA). Thirty days after injection, the mice were killed by an overdose of anaesthetic. The right sciatic nerve and L5 ventral and dorsal roots were dissected out. The L5 roots and DRG were pooled into one fraction corresponding to an axonal length of 12 mm. The sciatic nerve was cut into 3 mm consecutive segments starting from the L5 dorsal root ganglion to the muscular extremity.

Cloning

All *Als2* mRNA species were obtained by PCR amplification of the mouse *Als2* cDNA. PCR was performed on cDNA, generated from either brains of Als2$^{-/-}$ mice or WT littermate as described above, using the forward primer 5′- AGGCAGGAT CCTTTTCTCTAACACC -3′ and reverse primer 5′- CCCACC CCCACCCCTAGCAAAGTA -3′ for 40 cycles at 94°C for 30 s, 60°C for 30 s, and 72°C for 3.45 min. PCR product was cloned using TOPO TA cloning kit (Invitrogen). The cloned *Als2* PCR fragment was then subcloned into the zebrafish expression vector pCS2, donated by David Turner's laboratoty, between the *Cla*I site and the *Xba*I site of the multiple cloning sites. The cloned *Als2* PCR fragments were directly sequenced using the primers described above to confirm DNA sequences. *In vitro* synthesis of capped RNA was produced using Ambion SP6 mMESSAGE mMACHINE kit (cat# 1340).

Morpholino-mediated *zAls2* knock-down in zebrafish

The *Als2* zebrafish gene orthologue (*zAls2*) was identified using Ensembl's gene homology prediction program (http://www.ensembl.org, build Zv3). AMO (TGCACTCCTCCAT CCTCCGTCACGA) (Gene Tools, Oregon, USA) sequences were designed complimentary to the region of translational initiation (underlined) of the z*Als2* in order to inhibit protein translation. A control missense AMO was also tested and had the sequence (TcCACTgCTgCATCgTCCcTCACGA). AMO injections in 1–4 cell stage blastulae were performed as previously described (30). Zebrafish were raised from a colony maintained according to established procedures, and all procedures were carried out in compliance with the Canadian Council for Animal Care.

SUPPLEMENTARY MATERIAL

Supplementary Material is available at HMG Online.

ACKNOWLEDGEMENTS

The authors would like to thanks Pascale Hince, Janet Laganière, Roxanne Larivière, Sandra Laurent, Marie-Claude Richer, Daniel Rochefort, Mélanie Simard, Geneviève Soucy and Yuan-Chan Weng for technical assistance and helpful discussion.

Conflict of Interest statement. None declared.

FUNDING

This work was supported by the Canadian Institutes of Health Research, ALS Canada, the ALS Association (USA), The Robert Packard Center for ALS Research and the GRSNC of the Université de Montréal.

REFERENCES

1. Tandan, R. and Bradley, W.G. (1985) Amyotrophic lateral sclerosis: Part 1. Clinical features, pathology, and ethical issues in management. *Ann. Neurol.*, **18**, 271–280.
2. Mulder, D.W., Kurland, L.T., Offord, K.P. and Beard, C.M. (1986) Familial adult motor neuron disease: amyotrophic lateral sclerosis. *Neurology*, **36**, 511–517.
3. Pramatarova, A., Figlewicz, D.A., Krizus, A., Han, F.Y., Ceballos-Picot, I., Nicole, A., Dib, M., Meininger, V., Brown, R.H. and Rouleau, G.A. (1995) Identification of new mutations in the Cu/Zn superoxide dismutase gene of patients with familial amyotrophic lateral sclerosis. *Am. J. Hum. Genet.*, **56**, 592–596.
4. Rosen, D.R., Siddique, T., Patterson, D., Figlewicz, D.A., Sapp, P., Hentati, A., Donaldson, D., Goto, J., O'Regan, J.P., Deng, H.X. *et al.* (1993) Mutations in Cu/Zn superoxide dismutase gene are associated with familial amyotrophic lateral sclerosis. *Nature*, **362**, 59–62.
5. Hadano, S., Hand, C.K., Osuga, H., Yanagisawa, Y., Otomo, A., Devon, R.S., Miyamoto, N., Showguchi-Miyata, J., Okada, Y., Singaraja, R. *et al.* (2001) A gene encoding a putative GTPase regulator is mutated in familial amyotrophic lateral sclerosis 2. *Nat. Genet.*, **29**, 166–173.
6. Yang, Y., Hentati, A., Deng, H.X., Dabbagh, O., Sasaki, T., Hirano, M., Hung, W.Y., Ouahchi, K., Yan, J., Azim, A.C. *et al.* (2001) The gene encoding alsin, a protein with three guanine-nucleotide exchange factor domains, is mutated in a form of recessive amyotrophic lateral sclerosis. *Nat. Genet.*, **29**, 160–165.

7. Gros-Louis, F., Gaspar, C. and Rouleau, G.A. (2006) Genetics of familial and sporadic amyotrophic lateral sclerosis. *Biochim. Biophys. Acta.*, **1762**, 956–972.
8. Devon, R.S., Helm, J.R., Rouleau, G.A., Leitner, Y., Lerman-Sagie, T., Lev, D. and Hayden, M.R. (2003) The first nonsense mutation in alsin results in a homogeneous phenotype of infantile-onset ascending spastic paralysis with bulbar involvement in two siblings. *Clin. Genet.*, **64**, 210–215.
9. Eymard-Pierre, E., Lesca, G., Dollet, S., Santorelli, F.M., di Capua, M., Bertini, E. and Boespflug-Tanguy, O. (2002) Infantile-onset ascending hereditary spastic paralysis is associated with mutations in the alsin gene. *Am. J. Hum. Genet.*, **71**, 518–527.
10. Eymard-Pierre, E., Yamanaka, K., Haeussler, M., Kress, W., Gauthier-Barichard, F., Combes, P., Cleveland, D.W. and Boespflug-Tanguy, O. (2006) Novel missense mutation in ALS2 gene results in infantile ascending hereditary spastic paralysis. *Ann. Neurol.*, **59**, 976–980.
11. Gros-Louis, F., Meijer, I.A., Hand, C.K., Dube, M.P., MacGregor, D.L., Seni, M.H., Devon, R.S., Hayden, M.R., Andermann, F., Andermann, E. *et al.* (2003) An ALS2 gene mutation causes hereditary spastic paraplegia in a Pakistani kindred. *Ann. Neurol.*, **53**, 144–145.
12. Kress, J.A., Kuhnlein, P., Winter, P., Ludolph, A.C., Kassubek, J., Muller, U. and Sperfeld, A.D. (2005) Novel mutation in the ALS2 gene in juvenile amyotrophic lateral sclerosis. *Ann. Neurol.*, **58**, 800–803.
13. Panzeri, C., De Palma, C., Martinuzzi, A., Daga, A., De Polo, G., Bresolin, N., Miller, C.C., Tudor, E.L., Clementi, E. and Bassi, M.T. (2006) The first ALS2 missense mutation associated with JPLS reveals new aspects of alsin biological function. *Brain*, **129**, 1710–1719.
14. Cai, H., Lin, X., Xie, C., Laird, F.M., Lai, C., Wen, H., Chiang, H.C., Shim, H., Farah, M.H., Hoke, A. *et al.* (2005) Loss of ALS2 function is insufficient to trigger motor neuron degeneration in knock-out mice but predisposes neurons to oxidative stress. *J. Neurosci.*, **25**, 7567–7574.
15. Deng, H.X., Zhai, H., Fu, R., Shi, Y., Gorrie, G.H., Yang, Y., Liu, E., Dal Canto, M.C., Mugnaini, E. and Siddique, T. (2007) Distal axonopathy in an alsin-deficient mouse model. *Hum. Mol. Genet.*, **16**, 2911–2920.
16. Devon, R.S., Orban, P.C., Gerrow, K., Barbieri, M.A., Schwab, C., Cao, L.P., Helm, J.R., Bissada, N., Cruz-Aguado, R., Davidson, T.L. *et al.* (2006) Als2-deficient mice exhibit disturbances in endosome trafficking associated with motor behavioral abnormalities. *Proc. Natl. Acad. Sci. USA*, **103**, 9595–9600.
17. Hadano, S., Benn, S.C., Kakuta, S., Otomo, A., Sudo, K., Kunita, R., Suzuki-Utsunomiya, K., Mizumura, H., Shefner, J.M., Cox, G.A. *et al.* (2006) Mice deficient in the Rab5 guanine nucleotide exchange factor ALS2/alsin exhibit age-dependent neurological deficits and altered endosome trafficking. *Hum. Mol. Genet.*, **15**, 233–250.
18. Yamanaka, K., Miller, T.M., McAlonis-Downes, M., Chun, S.J. and Cleveland, D.W. (2006) Progressive spinal axonal degeneration and slowness in ALS2-deficient mice. *Ann. Neurol.*, **60**, 95–104.
19. Millecamps, S. and Julien, J.P. (2004) [35S]Methionine metabolic labeling to study axonal transport of neuronal intermediate filament proteins in vivo. *Methods Cell Biol.*, **78**, 555–571.
20. Marusich, M.F., Furneaux, H.M., Henion, P.D. and Weston, J.A. (1994) Hu neuronal proteins are expressed in proliferating neurogenic cells. *J. Neurobiol.*, **25**, 143–155.
21. Yeo, G., Holste, D., Kreiman, G. and Burge, C.B. (2004) Variation in alternative splicing across human tissues. *Genome Biol.*, **5**, R74.
22. Johnson, J.M., Castle, J., Garrett-Engele, P., Kan, Z., Loerch, P.M., Armour, C.D., Santos, R., Schadt, E.E., Stoughton, R. and Shoemaker, D.D. (2003) Genome-wide survey of human alternative pre-mRNA splicing with exon junction microarrays. *Science*, **302**, 2141–2144.
23. Otomo, A., Hadano, S., Okada, T., Mizumura, H., Kunita, R., Nishijima, H., Showguchi-Miyata, J., Yanagisawa, Y., Kohiki, E., Suga, E. *et al.* (2003) ALS2, a novel guanine nucleotide exchange factor for the small GTPase Rab5, is implicated in endosomal dynamics. *Hum. Mol. Genet.*, **12**, 1671–1687.
24. Topp, J.D., Gray, N.W., Gerard, R.D. and Horazdovsky, B.F. (2004) Alsin is a Rab5 and Rac1 guanine nucleotide exchange factor. *J. Biol. Chem.*, **279**, 24612–24623.
25. Tudor, E.L., Perkinton, M.S., Schmidt, A., Ackerley, S., Brownlees, J., Jacobsen, N.J., Byers, H.L., Ward, M., Hall, A., Leigh, P.N. *et al.* (2005) ALS2/Alsin regulates Rac-PAK signaling and neurite outgrowth. *J. Biol. Chem.*, **280**, 34735–34740.
26. Millecamps, S., Gentil, B.J., Gros-Louis, F., Rouleau, G. and Julien, J.P. (2005) Alsin is partially associated with centrosome in human cells. *Biochim. Biophys. Acta*, **1745**, 84–100.
27. Lesca, G., Eymard-Pierre, E., Santorelli, F.M., Cusmai, R., Di Capua, M., Valente, E.M., Attia-Sobol, J., Plauchu, H., Leuzzi, V., Ponzone, A. *et al.* (2003) Infantile ascending hereditary spastic paralysis (IAHSP): clinical features in 11 families. *Neurology*, **60**, 674–682.
28. Nagy, A., Rossant, J., Nagy, R., Abramow-Newerly, W. and Roder, J.C. (1993) Derivation of completely cell culture-derived mice from early-passage embryonic stem cells. *Proc. Natl. Acad. Sci. USA*, **90**, 8424–8428.
29. Gros-Louis, F., Lariviere, R., Gowing, G., Laurent, S., Camu, W., Bouchard, J.P., Meininger, V., Rouleau, G.A. and Julien, J.P. (2004) A frameshift deletion in peripherin gene associated with amyotrophic lateral sclerosis. *J. Biol. Chem.*, **279**, 45951–45956.
30. Nasevicius, A. and Ekker, S.C. (2000) Effective targeted gene 'knockdown' in zebrafish. *Nat. Genet.*, **26**, 216–220.